Supplementary Information

Floating under a levitating liquid

Authors: Benjamin Apffel, Filip Novkoski, Antonin Eddi, Emmanuel Fort

Correspondence to: emmanuel.fort@espci.fr

Supplementary Models

1. Sinking bubbles in a vibrating bath
2. Spring-mass model for the levitating liquid layer
3. Stabilization of an inverted liquid/air interface by vertical oscillations
4. Dynamical stabilization of floating bodies at the lower and upper interface of a levitated oscillating liquid layer

Supplementary Raw Data

Supplementary Models

1. Sinking bubbles in a vibrating bath

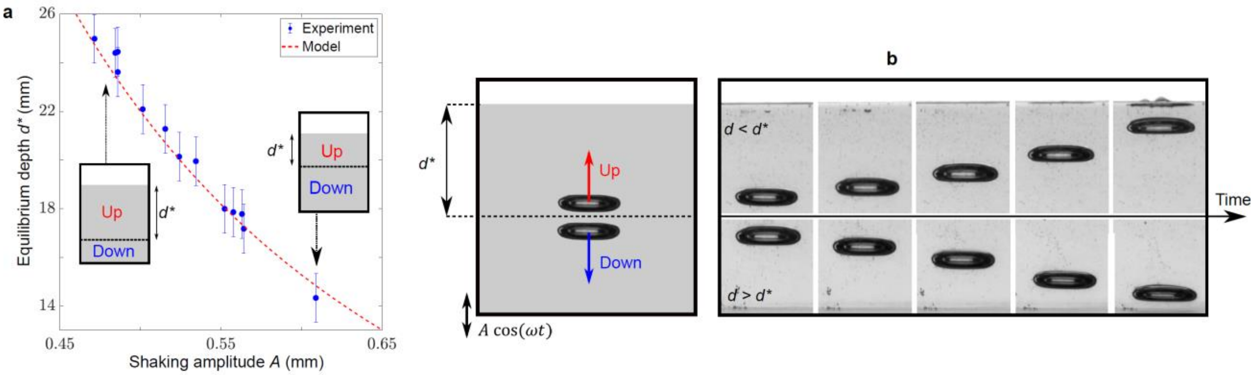

Figure S1 Sinking bubbles in a vibrated bath a, Evolution of the critical sinking depth d^* as a function of the shaking amplitude A. Data are fitted by an invert quadratic scaling c/A^2 with $c = 5.5$ mm^3. The error bars are taken as half of the height of the bubble. **b**, Schematics and image sequence of an ascending and descending bubble produced respectively above and below the critical sinking depth d^* (see Supplementary Video 1).

We consider a tank filled with liquid of density ρ_l vibrated vertically at frequency $\omega/2\pi$ with an amplitude A (Fig. S1a). Air bubbles are created at various depths d using a long needle connected to a syringe. Bubbles are observed to sink when placed below a critical depth d^*, while they reach the upper surface if created above d^* (see snapshots Fig. S1b and Supplementary Video 1). This behavior which defies standard buoyancy can be understood by a simple model taking into account the kinetic force exerted on the bubble in the oscillating bath[14,16].

In a still bath, the buoyant force results from the difference in pressure between the top and bottom of the bubbles. This creates a constant upward force given by $F = \rho_l V g$ with g the gravitational acceleration, V the volume of the body and ρ_l the density of the fluid. In the oscillating bath, the effective gravity is modulated following $g_{\mathrm{eff}}(t) = g + \gamma_{\mathrm{exc}}(t)$ with $\gamma_{\mathrm{exc}}(t) = -A\omega^2\cos(\omega t)$ the bath acceleration. In addition, in the case of an air bubble at depth d, the pressure modulation induces a volume modulation $V(t)$ which can be considered isothermal and quasi-static for the low frequencies used (typically 100 Hz). The volume oscillations satisfy $V(t) = V_0 P_0/P(t)$ with $P(t)$ the gas pressure satisfying $P(t) = P_{\mathrm{atm}} + \rho_l g_{\mathrm{eff}}(t) d$ with P_{atm} being the atmospheric pressure and the index 0 standing for the values at rest ($P_0 = P_{\mathrm{atm}} + \rho_l g d$). Assuming that the pression modulation is small compared to P_{atm}, one can perform a Taylor development of the volume as $V(t) = V_0(1 - \frac{\rho_l \gamma_{\mathrm{exc}}(t) d}{P_0})$. By averaging the force $F = \rho_l V(t) g_{\mathrm{eff}}(t)$ over one oscillation period we get $F = \rho_l g V_0 - \frac{\rho_l^2 A^2 \omega^4 V_0 d}{2P_0}$ so that an additional sinking force, called the Bjerknes force [30], arises.

Below a critical depth $d^*_{\mathrm{th}} \approx 2gP_0/(\rho_l A^2 \omega^4)$ corresponding to the equilibrium, the bubbles sink [14–16].

Figure S1a shows d^* as a function of the shaking amplitude A in good agreement with an adjusted inverted quadratic scaling $1/A^2$. The fit parameter is a characteristic volume that can be written as $c = \frac{P_0}{\rho_l \omega^2} \frac{2g}{\omega^2}$, the first term being associated with the square of the radius of an air bubble of resonant frequency ω representing the modulation of its volume[14,15], and the second one being a characteristic length coming from the effect of gravity on the bubble via the column of liquid above. The critical depth was measured by placing the bubble at the critical point (that we can tune by changing the amplitude of shaking), which serves as an equilibrium. We then took short videos to determine the amplitude of the shaking and the average position of the center of mass of the bubble with respect to the surface. The gas that was injected was simply air from the surroundings, at room temperature and humidity.

The very existence of such a depth d^* is a result of a π-shift between the volume oscillations and the effective gravity ones. More complete models taking other aspects of the problem into account, such as sound waves in the fluid, type of gas in the bubble, compressibility of the liquid due to the presence of small air bubbles and the size of the bubble itself, can be found in [15–17,19,20,34].

2. Spring-mass model for the levitating liquid layer

We consider a liquid layer maintained above a layer of air by shaking vertically. In the laboratory frame, the position of the bottom interface of the air layer moves with the container and satisfies $z_b(t) = A\cos(\omega t + \phi)$ with A, ω and ϕ being the amplitude, the angular frequency and the phase of the forcing. The position of the upper interface of the air layer is given by $z_l(t)$. The height of the air layer is thus given by $z_a(t) = z_l(t) - z_b(t)$. This corresponds also to the relative motion of the upper interface, and thus of the levitating liquid layer relative to the container (see Figure S2).

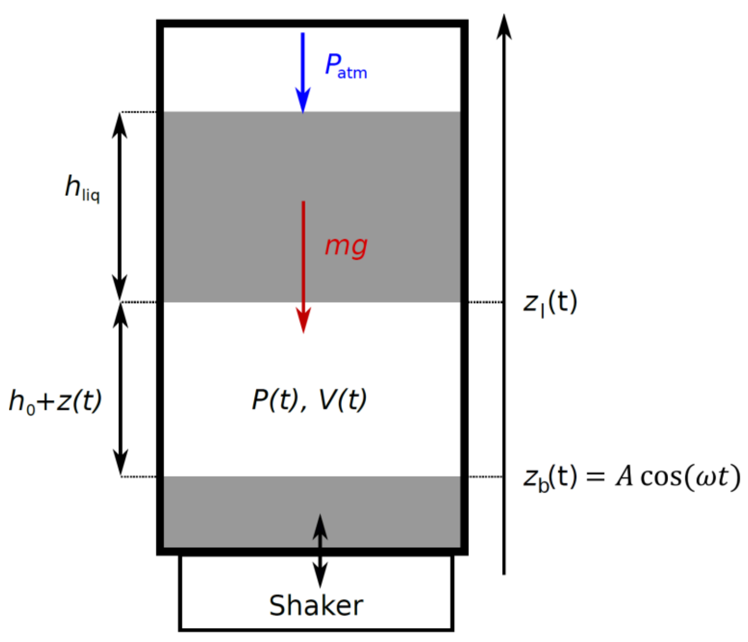

Figure S2 Sketch of a levitating liquid layer with notations

The air layer is considered as a perfect gas and its pressure $P(t)$and volume $V(t)$are assumed to verify:

$$P(t)V(t)^{\beta} = P_0 {V_0}^{\beta} \tag{1}$$

with β being the polytropic index, P_0 and $V_0$the static pressure and volume respectively. In addition,$P_0 = P_{\text{atm}} + mg/S$, m being the mass of the levitating liquid layer and $V_0 = Sh_0$, h_0 being the height of the air layer at rest. Depending on the transformation the value of β can var: $\beta = 1$for an isothermal process while $\beta$is equal to the heat capacity ratio for an adiabatic one.

For small oscillations observed experimentally around the mean height h_0, we can perform a Taylor expansion of eq. (1) and get the pressure in the gas as

$$P(t) \approx\ P_0(1 - \beta z(t)/h_0) \tag{2}$$

With $z(t) = z_{\text{a}}(t) - h_0 \ll h_0$ for small oscillations. Writing the Newton's law for the liquid layer, we obtain

$$m\ddot{z}_{\text{l}} = -mg - SP_{atm} + SP_0(1 - \frac{\beta z}{h_0}) - c\dot{z} \tag{3}$$

with c coming from damping.

On the right-hand side of the equation, the first term is the weight of the liquid layer, the second and third terms result from the air pressure on both sides of the liquid layer and the fourth term is damping due to the relative motion between the container and the liquid.

This can be rewritten as a damped harmonic oscillator with a sinusoidal forcing (as in the paper)

$$\ddot{z} + 2\mathit{\Gamma}\omega_{\text{res}}\dot{z} + \omega_{\text{res}}^2 z = -\ddot{z}_b \tag{4}$$

with the resonant frequency satisfying $\omega_{\text{res}}^2 = \beta P_0 S/mh_0$ and the damping ratio $\mathit{\Gamma} = \frac{\text{c}}{2m\omega_{\text{res}}}$ Hence the motion of the liquid in the laboratory frame writes $z_{\text{l}}(t) = A_{\text{l}}\cos(\omega t + \phi_{\text{l}})$.

We finally have, with $\widehat{\omega} = \omega/\omega_{\text{res}}$, for the relative amplitude

$$\frac{A_{\text{l}}}{A} = \sqrt{\frac{1+4\mathit{\Gamma}^2\widehat{\omega}^2}{(1-\widehat{\omega}^2)^2+4\mathit{\Gamma}^2\widehat{\omega}^2}} \tag{5}$$

and for the relative phase

$$\phi_l - \phi = \text{atan}\, 2\mathit{\Gamma}\widehat{\omega} - \text{atan}\frac{2\mathit{\Gamma}\widehat{\omega}}{1-\widehat{\omega}^2} \tag{6}$$

These expressions were used to produce the fits in Fig. 1c and 1d respectively. We obtain for the damping ratio $\Gamma \approx 0.04$ and for $\omega_{\text{res}}/2\pi \approx 103$ Hz. The experimental conditions give $h_0 \approx 1.5$ cm and the liquid layer height $h_{\text{l}} \approx 2.5$ cm. Using these values and the glycerol density $\rho = 1.1$ kg/L, we can estimate $\beta \approx 1.7$. This value is slightly higher than expected, one would rather expect a value in the range $1 \leq \beta \leq 1.4$ between an isothermal transformation and an adiabatic one.

3. Stabilization of an inverted liquid/air interface by vertical oscillations

We focus our attention on the evolution of small perturbations at the interface of two incompressible and immiscible fluids. ρ_{up} and ρ_{down} are the densities of the upper and lower fluids respectively. The interface is placed at $z = 0$ and the perturbations at position $\boldsymbol{r}$and time $t$in the horizontal plane are $\zeta(\boldsymbol{r}$,t).

It is convenient to study the interface deformations in the spatial Fourier space, $\zeta(\boldsymbol{k})$ is the deformation at the spatial frequency $k = |\boldsymbol{k}|$ and in the direction $\boldsymbol{k}$**.**

Assuming the fluid velocities at the interface are small, it is possible to linearize Bernoulli's equations and show that each interface deformation $\zeta(\boldsymbol{k})$ behaves as a harmonic oscillator [32]

$$\ddot{\zeta}(\boldsymbol{k}) + \omega_0(k)^2\zeta(\boldsymbol{k}) = 0 \qquad (7)$$

with the angular frequency $\omega_0(k)$ satisfying the dispersion relation $\omega_0(k)^2 = -Agk + \gamma k^3/(\rho_{\text{up}} + \rho_{\text{down}})$,$g$ the gravitational acceleration, γ the surface tension and $A = (\rho_{\text{up}} - \rho_{\text{down}})/(\rho_{\text{up}} + \rho_{\text{down}})$ is the Atwood number.

We now consider the standard configuration with a liquid of density ρ_{l} and the air interface above. Neglecting the density of air, $\omega_0(k)^2 = gk + \gamma k^3/\rho_{\text{l}}$ which is the standard gravity-capillary dispersion relation[33]. In this case, both gravity effects and capillary ones are positive and thus stabilize the interface resulting in the propagation of waves along the interface.

We now assume that the liquid stands above the air i.e. we turn the previous interface upside down. In this case the dispersion relation writes: $\omega_0(k)^2 = -gk + \gamma k^3/\rho_{\text{l}}$. The effect of the gravity on the interface is reversed while capillarity is not affected. The gravity term is negative inducing a destabilization of the interface.

For small wave vectors for which gravity effects dominate, $\omega_0(k)^2 < 0$ so that a perturbation of the interface will exponentially increase in time and the liquid will eventually fall down. We recover here the well-known Rayleigh-Taylor instability that occurs when a heavier fluid is set above a lighter one. The most unstable mode occurs for the minimum (negative) value of $\omega_0(k)^2$ which is associated to the wavenumber $k = \sqrt{\rho g/3\gamma}$. For large wave vectors, capillarity dominates and it has a stabilizing effect.

We are now focusing on dynamical stabilization induced by vertical vibrations of the fluid.

We assume that the liquid is submitted to a vertical oscillation $A_l \cos(\omega t)$. The acceleration of the liquid is then $-A_l\omega^2 \cos(\omega t)$. The acceleration of the liquid can be interpreted as a modulation of the effective gravity $g_{\mathrm{eff}}(t) = g - A_l\omega^2 \cos(\omega t)$in the accelerated frame.

Eq. (7) can thus be modified using g_{eff} and we obtain

$$\ddot{\zeta} + \omega_0(k)^2\zeta = -kA_l\omega^2 \cos(\omega t)\,\zeta \tag{8}$$

We now perform an analysis similar to the one used by Kapitza[7,31] for the stabilization of the inverted pendulum shaken vertically[31]. We decompose ζinto a slow component $\zeta_s$and a fast one ζ_f oscillating at ω so that $\zeta = \zeta_s + \zeta_f$. This decomposition is justified for k modes satisfying $|\omega_0(k)| \ll \omega$. In this case, the evolution of the height $\zeta(\boldsymbol{k})$is slow compared to the modulation. For all unstable modes, this hypothesis is well verified in our experimental conditions.

We can then expect that the vibration will induce a slow additional stabilizing effect on $\zeta_s$induced by a fast perturbation ζ_f at angular frequency ω. We denote with <.> the mean over one oscillation period. We have $<\zeta_f> = 0$ and $<\zeta_s \cos(\omega t)> = 0$. Writing the equation of motion and keeping only terms oscillating at ω and first order term in ζ_f gives $\ddot{\zeta}_f \approx -kA_l\omega^2 \cos(\omega t)\,\zeta_s$ so that $\zeta_f \approx kA_l \cos(\omega t)\,\zeta_s$. We now take the mean <.> of the evolution eq. (8) and get:

$$\ddot{\zeta}_s + \omega_0(k)^2\zeta_s = -kA_l\omega^2 < \cos(\omega t)\,\zeta_f > = -\frac{k^2A_l^2}{2}\omega^2\zeta_s \tag{9}$$

Or equivalently

$$\ddot{\zeta} + \left[\omega_0(k)^2 + \frac{A_l^2k^2}{2}\omega^2\right]\zeta = 0 \tag{10}$$

We recover here the equation given in the main text and find that the new dynamical term resulting from the vibration is positive and thus tends to stabilize the interface.

This equation is valid as long as $|\omega_0(k)| \ll \omega$. For large wave vectors, $|\omega_0(k)| \ll \omega$ does not hold anymore, however these modes are stabilized by capillarity ($\omega_0(k)^2 > 0$). For the unstable modes with small k for which $\omega_0(k)^2 < 0$, the condition $|\omega_0(k)| \ll \omega$ can always be satisfied. The condition to stabilize a mode with a given $k$is given by $k > \frac{2g}{A_l^2\omega^2}$.
Hence, for an interface of size L, the excitable wavenumbers satisfy $k > \pi/L$, and one has to apply an excitation velocity $v_l = A_l\omega > \sqrt{2gL/\pi}$.

Note that in the experiments, the air layer trapped under the liquid tends to mute the anti-symmetric modes on the interface ($k = \pi q/L$ with q being an odd number). These modes do not conserve the volume of the air layer. The stability of an interface of length L in this case should satisfy $v_l = A_l\omega > \sqrt{gL/\pi} = v_l^*$ as measured experimentally (see Fig. 1f).

Other effects might have an influence on the stability, such as friction or the flows formed at the boundary. By a simple order of magnitude estimate, we can judge the effect of friction through viscosity through the force $F = S\sigma_{xz}$ where S is the area and σ_{xz} the stress tensor. By using the values found in our system, we obtain a force of order 10^{-3} N, which compared to the mass of the layer is negligible. The vortices at the boundaries which are visible in the supplementary Videos can have a possible effect near resonance since they appear due to relative motion of liquid and container, but at low frequencies the layer is still stable despite the vortices being much weaker.

4. Dynamical stabilization of floating bodies at the lower and upper interface of a levitated oscillating liquid layer

a. Dynamical effects on floating bodies on the vibrated liquid interface

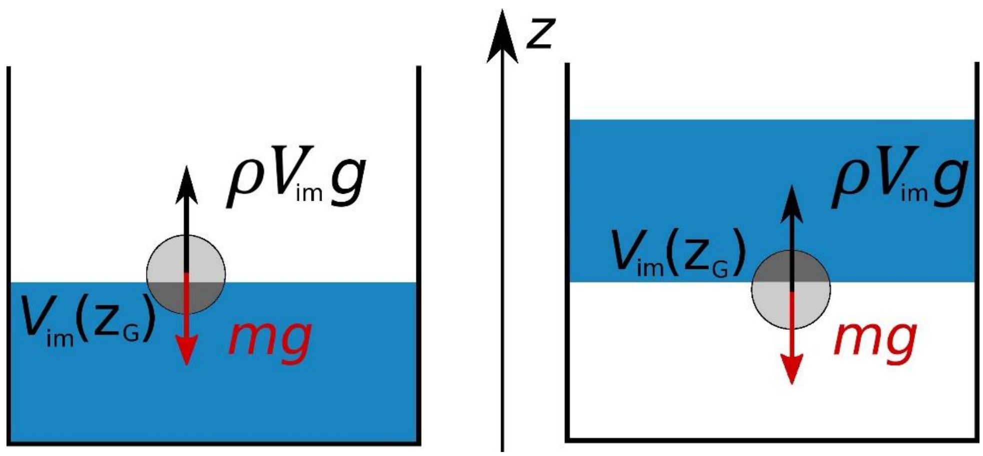

Figure S3 Sketches of the floating equilibrium on the upper interface and on the inverted interface

We consider a body of mass m_b, volume V_b and density $\rho_\mathrm{b} = m_\mathrm{b}/V_\mathrm{b}$ floating on a bath of liquid of higher density$\rho_\mathrm{l} > \rho_\mathrm{b}$. The capillary effects are neglected.

The buoyant force is due to hydrostatic pressure in the liquid, and it satisfies

$$\boldsymbol{F}_\mathrm{b} = -\int_S P d\boldsymbol{S} = -\int_V \boldsymbol{\nabla} P dV = \rho_\mathrm{l} g V_\mathrm{im}(z_\mathrm{G}) \qquad (11)$$

With P the pressure exerted on the body surface S, V is the body volume and $V_\mathrm{im}(z_\mathrm{G})$ is the immersed volume with the center of mass at vertical position z_G (see Fig. S3). We consider that the immersed volume is fully characterized by z_G i.e. it does not depend on the orientation of the body and the center of pressure coincides with the center of mass, or it is determined for a given body orientation if the center of pressure is different from the center of mass. In the latter case, the stable orientation is obtained for the center of pressure positioned above the center of mass.

By applying Newton's second law, we readily obtain the natural frequency of a floating body oscillating around a stable equilibrium at height $z_\mathrm{G,eq}$

$$\omega_\mathrm{b}^2 = -\frac{\rho_\mathrm{l} g}{m_\mathrm{b}} \frac{dV_\mathrm{im}}{dz}\left(z_\mathrm{G,eq}\right) > 0 \qquad (12)$$

For a sphere of radius 1 cm in glycerol being half submerged one has $\omega_\mathrm{b} \simeq 40$ rad/s.

We now focus on the effect of an added vertical acceleration of the liquid with angular frequency ω and amplitude A on the equilibrium position. In this case the liquid is submitted to an oscillating effective gravity $g_\mathrm{eff}(t) = g - A\omega^2\cos(\omega t)$ with the proper choice of the time origin.

In the low excitation frequency range used in the experiment ($\omega/2\pi < 150$ Hz), the hydrostatic pressure in the liquid and the constant atmospheric pressure outside still holds. The buoyant force is thus given by eq. (11) using the effective gravity: $F_\mathrm{b} = \rho_\mathrm{l} g_\mathrm{eff} V_\mathrm{im}(z_\mathrm{G})$.

To write Newton's second law, we assume that the floating body moves with the liquid and that there is no relative motion between the body and the surrounding liquid. This hypothesis is verified by experimental observations. Under this assumption, the equation of motion in the accelerated frame is given by eq. (12) using the effective gravity

$$m_\mathrm{b}\ddot{z_\mathrm{G}} = -m_\mathrm{b} g_\mathrm{eff} + \rho_\mathrm{l} g_\mathrm{eff} V_\mathrm{im}(z_\mathrm{G}) \qquad (13)$$

The equilibrium position is the same as for the static liquid. Following the previous analysis for small displacements Z around the equilibrium position, we obtain

$$\ddot{Z} + \omega_\mathrm{b}^2 Z = \omega_\mathrm{b}^2 \frac{A\omega^2}{g}\cos(\omega t) Z \qquad (14)$$

We now assume that $\omega_\mathrm{b} \ll \omega$ which is always verified in our experimental cases and we use Kapitza's approach for the dynamical stabilization of an inverted pendulum using vertical shaking[31,32]. We decompose Z into a slow component Z_s and a fast one Z_f at the excitation frequency ω so that $Z = Z_\mathrm{s} + Z_\mathrm{f}$. Denoting $<.>$ the mean value over the excitation period, the two components satisfy $< Z_\mathrm{s}\cos(\omega t) >= 0$ and $< Z_\mathrm{f} >= 0$. Under these conditions, we find for the oscillating terms at ω at first order in Z_f [33]

$$\ddot{Z}_\mathrm{f} = \omega_\mathrm{b}^2 \frac{A\omega^2}{g}\cos(\omega t)\, Z_\mathrm{s} \qquad (15)$$

Hence,

$$Z_\mathrm{f} = -\omega_\mathrm{b}^2 \frac{A}{g}\cos(\omega t)\, Z_\mathrm{s} \qquad (16)$$

Averaging eq. (14) over an excitation period and using eq. (16), we obtain

$$\ddot{Z}_\mathrm{s} + \omega_\mathrm{b}^2 Z_\mathrm{s} = -\frac{\omega_\mathrm{b}^4}{2}\left(\frac{A\omega}{g}\right)^2 Z_\mathrm{s} \qquad (17)$$

This gives

$$\ddot{Z}_s + \omega_b^2(1+\alpha)Z_s = 0 \qquad \text{with } \alpha = \frac{\omega_b^2}{2}\left(\frac{A\omega}{g}\right)^2 \tag{18}$$

The term α is a dynamical term resulting from the non-zero correlation between the floating object motion and the modulated pressure due to the vibration. Since $\alpha > 0$, this term induces an additional stabilization of the equilibrium floating position (see Fig. 2b).

b. Dynamical stabilization of floating bodies on the lower interface of a levitating liquid

We consider the case of the lower interface in a levitating liquid layer (see Fig. S3). The liquid layer is stabilized by vertical oscillations with an amplitude A_l and an angular frequency ω. We assume that such an inverted interface exists and is stable regardless of its underlying stabilization mechanism induced by the vibration.

We first focus on the existence of a static equilibrium at each interface. Under the hypothesis of a hydrostatic pressure in the liquid and a constant pressure in the trapped air layer, the static equation (12) still applies. Two equilibrium positions can thus be found for a floating body, both satisfying eq. (13). The standard equilibrium on the upper interface and another equilibrium on the lower interface (see Fig. 2b).

As an object is moved through the lower interface, its immersed volume V_im varies from the entire body volume to zero (when entirely in the air layer). Hence, the symmetric equilibrium positions on the two interfaces satisfying $V_\mathrm{im}(z_\mathrm{G,eq}) = m_\mathrm{b}/\rho_\mathrm{l}$ are equilibrium positions.

However, for the lower interface, this position is not stable, pushing the body slightly upward, increases the immersed volume and results in a net upward force while pushing the body downward reduces the immersed volume and makes the body fall.

This originates from the positive sign of $\frac{dV_\mathrm{im}}{dz} > 0$ for the lower interface which results in a negative sign for $\omega_\mathrm{b}^2 = -\frac{\rho_\mathrm{l} g}{m_\mathrm{b}}\frac{dV_\mathrm{im}}{dz}\left(z_\mathrm{G,eq}\right) < 0$.

Taking into account the vertical oscillations and following the same approach as in the previous section leads to the same eq. (15). For small displacements Z around the lower equilibrium position with a fast dynamic Z_f and a slow one Z_s, one obtains

$$\ddot{Z}_s + \omega_b^2(1+\alpha)Z_s = 0 \qquad \text{with} \quad \alpha = \frac{\omega_b^2}{2}\left(\frac{A_\mathrm{l}\omega}{g}\right)^2 \tag{19}$$

However, now $\omega_\mathrm{b}^2 < 0$ and thus $\alpha < 0$.

The equilibrium is stable if $\omega_\mathrm{b}^2(1+\alpha) > 0$ which is possible if $\alpha < -1$.

One obtains the following stability condition for the amplitude of the forcing velocity

$$A_{\mathrm{l}}\omega > \frac{\sqrt{2}g}{|\omega_{\mathrm{b}}|} = v_{\mathrm{l}} \tag{20}$$

Note that for objects with a non-coincident center of pressure and center of mass, the former should always be above the latter for stability. However, experimentally an equilibrium is easily found even in the opposite orientation of the body (see Fig. 2e).

We can also evaluate the consequences of the secondary flow (see Fig. 1b and Video 2) on the floating object by estimating the drag force on the floater. From the video, we have $V \approx 1$ cm/s and a floater of size $R \approx 1$ cm, and thus a Reynolds number $Re \approx 0.3$. This means that viscous effects (slightly) dominate in this flow. From this we deduce the viscous drag force $F_{\mathrm{v}} \approx \eta RV \approx 5.10^{-5}$ N, much smaller than the weight of the floater 10^{-2} N. The secondary flow should thus not significantly change the vertical equilibrium of the floaters.

To match with notation of Figure 2, we describe briefly the previous situation in terms of potential energy. We first assume no forcing. When the object is only in one fluid (than can be air or liquid) of density ρ, the strength applied is constant so the energy will be linear with respect to the z-coordinate $E_p = (m_{\mathrm{b}} - \rho V_{\mathrm{b}})gz$. When the object crosses the interface between air and liquid the exact profile of the potential will depend on the exact shape of the object. More precisely, it will be a primitive of $m_{\mathrm{b}} g_{\mathrm{eff}} - \rho_{\mathrm{l}} g_{\mathrm{eff}} V_{\mathrm{im}}(z)$ if we neglect density of the air in front of the density of the liquid. Assuming the object floats (that means $m_b < \rho_{\mathrm{l}} V_{\mathrm{b}}$) there will be an extremum to this primitive that corresponds to the position $z_{\mathrm{G,eq}}$where weight and buoyancy cancel each other out. At first order the energy will be a parabola around this point and the orientation of the parabola (and so the stability of the system) will depend on the sign of $\omega_{\mathrm{b}}^2 = -\frac{\rho_{\mathrm{l}} g}{m_{\mathrm{b}}} \frac{dV_{\mathrm{im}}}{dz}\left(z_{\mathrm{G,eq}}\right)$. The junction between this parabola and the linear potential found before will depend on the shape of the object. For simple objects such as a cube or a sphere, it qualitatively looks like the plot presented in figure 2b. As expected, the upper position is stable while the lower one is not.

We now add a vertical forcing and aim to find the potential energy for the slow variable. When the object does not cross the interface, the potential energy remains the same linear function. However, around the extrema, it has been shown that the vibration adds an extra force (see eq. 19) that will appear as an additional parabolic term in the potential energy. At the upper interface this term will make the equilibrium position even more stable while the lower position can be stabilized if the forcing is high enough (see Fig. 2b). Note that this approach is only valid around the equilibrium position. The junction between the linear potential and the parabolas (if any exist) would require further investigation and hence are not represented on the plots.

Supplementary: Raw data

Raw data used to plot the figures presented in the paper. When several measurements are made in the same configuration, a slash symbol "/" separates the different results obtained.

Figure 1d

f (Hz)	A_l (a.u.)	A (a.u.)	A_l/A	$\phi_l - \phi$ (rad)
80	24.9793	5.7567	4.33917001	-0.2914
81	23.79	5.5789	4.26428149	-0.379
82	22.9815	5.3718	4.27817491	-0.485
83	22.3235	5.2104	4.28441195	-0.5492
84	24.582	4.718	5.21025858	-0.362
85	22.2967	4.5493	4.90112765	-0.5419
86	22.7991	4.0264	5.66240314	-0.3555
87	23.047	3.9033	5.90449107	-0.3815
88	22.1788	3.7487	5.91639768	-0.4997
89	21.1037	3.2117	6.57088146	-0.4262
90	21.2632	3.0897	6.88196265	-0.4369
91	21.5839	2.9764	7.25167988	-0.4713
92	21.9778	2.8822	7.62535563	-0.5195
93	21.0605	2.7485	7.66254321	-0.6581
94	19.4971	2.6643	7.31790714	-0.8418
95	19.2479	2.3808	8.08463542	-0.8067
96	19.7263	2.1423	9.20800075	-0.8185
97	19.8222	1.9394	10.2207899	-0.8186
98	17.9493	1.8753	9.57142857	-1.0775
99	17.0939	1.7988	9.50294641	-1.465
100	17.3981	1.7031	10.2155481	-1.6626
101	16.8518	1.5952	10.5640672	-1.8485
102	16.8269	1.3839	12.1590433	-1.5567
103	16.643	1.326	12.5512821	-1.7458
104	16.5409	1.2784	12.9387516	-1.7892
105	16.1355	1.3555	11.9037256	-2.103
106	15.9497	1.4084	11.3246947	-2.2236
107	15.7071	1.4696	10.6880103	-2.1942
108	15.2729	1.6175	9.44228748	-2.4026
109	14.8581	1.7486	8.49714057	-2.4269
110	14.5351	1.875	7.75205333	-2.5679
111	13.5258	1.9345	6.99188421	-2.5584
112	13.6042	2.0399	6.6690524	-2.5795
113	13.2577	2.1955	6.03857891	-2.6169

114	12.9526	2.3675	5.47100317	-2.6703
115	12.7711	2.4619	5.18749746	-2.7071
116	12.2187	2.6484	4.61361577	-2.7348
117	12.0951	2.7923	4.33159045	-2.7704
118	12.223	3.0052	4.06728338	-2.8582
119	12.3384	3.0791	4.00714494	-2.8461
120	11.868	3.3795	3.51176209	-2.947
121	11.4123	3.5017	3.25907416	-2.921
122	10.9166	3.5981	3.03399016	-2.9645
123	10.9271	3.7931	2.88078353	-2.9737
124	11.2063	3.8164	2.93635363	-2.9341
125	10.193	4.0513	2.51598252	-3.0381
126	10.0196	4.1587	2.4093106	-3.0034
127	8.6268	4.4318	1.94656799	-3.1006
128	10.1349	4.3799	2.31395694	-2.9687
129	8.5261	4.6164	1.84691535	-3.0713
130	7.6751	4.7395	1.61939023	-2.9524

Figure 1f

The position of the liquid is defined as $A_l \cos(\omega t)$, and the critical velocity is $v_l^* = A_l^* \omega$. We measured peak-to-peak critical amplitude of the position of the center of the layer $2A_l^*$ and deduced v_l^*. The uncertainty δv_l^* takes into account dispersion of data over several measurements.

L (cm)	$2A_l^*$ (mm)	Frequency (Hz)	v_l^* (m/s)	δv_l^* (m/s)
2	1.2/1.2/1.1/1.1/1.1	100	0.36	0.05
5	2/2.1/1.7/2.1/2	80	0.5	0.15
7	1.7/1.4/1.5/1.5/1.6/1.8	100	0.5	0.1
10	2.5/2.6/2.4	80	0.63	0.1
14	2.7/2.9/3/ 2.7/2.6/2.9	80	0.7	0.05
18	2.7/2.8/3.2/3.1/3	80	0.74	0.05

Figure 2d

In each case (static/upper interface/lower interface) the figure given is the distance in millimeter between the emerged top of the sphere and the interface (respectively $h_{rest}, h_{up}, h_{down}$). We then deduce the associated immersed volume. The uncertainties take into account dispersion of data over several measurements.

m_b (g)	h_{rest} (mm)	h_{up} (mm)	h_{down} (mm)	V_{rest} (cm³)	δV_{rest} (cm³)	V_{up} (cm³)	δV_{up} (cm³)	V_{down} (cm³)	δV_{down} (cm³)
0.8	14	15	14.5	0.9	0.08	0.65	0.1	0.78	0.11

1.1	13	12.5	13	1.18	0.09	1.33	0.13	1.18	0.13
1.4	12	12.5/13	14	1.47	0.09	1.33	0.13	0.9	0.12
1.7	10	11.5	12.5	2.1	0.1	1.63	0.14	1.33	0.13
2.1	9	11	12.5/11	2.41	0.1	1.78	0.14	1.47	0.13
2.4	9	10	11.5/10	2.41	0.1	2.1	0.14	1.78	0.14
2.7	8	10	11/12	2.71	0.1	2.1	0.14	1.78	0.14
3	7	10	10/8.5	3.15	0.09	2.1	0.14	2.25	0.14
4.1	5.5	6.5	6.5/7.5/8	3.41	0.08	3.15	0.13	2.86	0.13
4.4	3.5	4/4.5/6	7.5	3.85	0.06	3.41	0.12	2.86	0.13

Figure 3

Frequency of shaking is 80 Hz. Critical velocities are defined as $v_l^* = A_l^* \omega$ and $v_f^* = A_f^* \omega$. We measured peak-to-peak amplitude of the position of the center of the layer $2A_l$. For light floaters ($m_b < 5\ g$) the entire layer falls when $A_l = A_l^*$. These floaters were not observed to fall alone. For heavy floaters ($m_b > 5\ g$) the floater falls alone for $A_l = A_f^*$ and the liquid falls for $A_l = A_l^*$. The uncertainties take into account dispersion of data over several measurements.

m_b (g)	$2A_l^*$	$2A_b^*$	v_l^*	δv_l^*	v_f^*	δv_f^*
3.2	2.1/2.2	-	0.53	0.05	-	-
4.2	2.4/2.1/2.2	-	0.58	0.05	-	-
4.8	2.1/2.2/2.5	-	0.55	0.05	-	-
5.5	2.2/2.1/2.1/2.1	2.1	0.55	0.05	0.55	0.05
6	2.2/2.3/2.3/2.3	2.4/2.3	0.53	0.05	0.58	0.05
6.65	2.2/2.1/2.1	2.3/2.3/2.4	0.55	0.05	0.58	0.05
7	2/2.2	2.8/2.4	0.53	0.05	0.65	0.08
7.35	2.2/2.3/2.1	2.5/2.5/2.4	0.53	0.05	0.63	0.05